JACS
JOURNAL OF THE AMERICAN CHEMICAL SOCIETY

Subscriber access provided by Uppsala universitetsbibliotek

Article

Efficient C-H amination catalysis using nickel-dipyrrin complexes

Yuyang Dong, Ryan M. Clarke, Gerard J. Porter, and Theodore A. Betley

J. Am. Chem. Soc., **Just Accepted Manuscript** • Publication Date (Web): 27 May 2020

Downloaded from pubs.acs.org on May 28, 2020

Just Accepted

"Just Accepted" manuscripts have been peer-reviewed and accepted for publication. They are posted online prior to technical editing, formatting for publication and author proofing. The American Chemical Society provides "Just Accepted" as a service to the research community to expedite the dissemination of scientific material as soon as possible after acceptance. "Just Accepted" manuscripts appear in full in PDF format accompanied by an HTML abstract. "Just Accepted" manuscripts have been fully peer reviewed, but should not be considered the official version of record. They are citable by the Digital Object Identifier (DOI®). "Just Accepted" is an optional service offered to authors. Therefore, the "Just Accepted" Web site may not include all articles that will be published in the journal. After a manuscript is technically edited and formatted, it will be removed from the "Just Accepted" Web site and published as an ASAP article. Note that technical editing may introduce minor changes to the manuscript text and/or graphics which could affect content, and all legal disclaimers and ethical guidelines that apply to the journal pertain. ACS cannot be held responsible for errors or consequences arising from the use of information contained in these "Just Accepted" manuscripts.

is published by the American Chemical Society. 1155 Sixteenth Street N.W., Washington, DC 20036

Published by American Chemical Society. Copyright © American Chemical Society. However, no copyright claim is made to original U.S. Government works, or works produced by employees of any Commonwealth realm Crown government in the course of their duties.

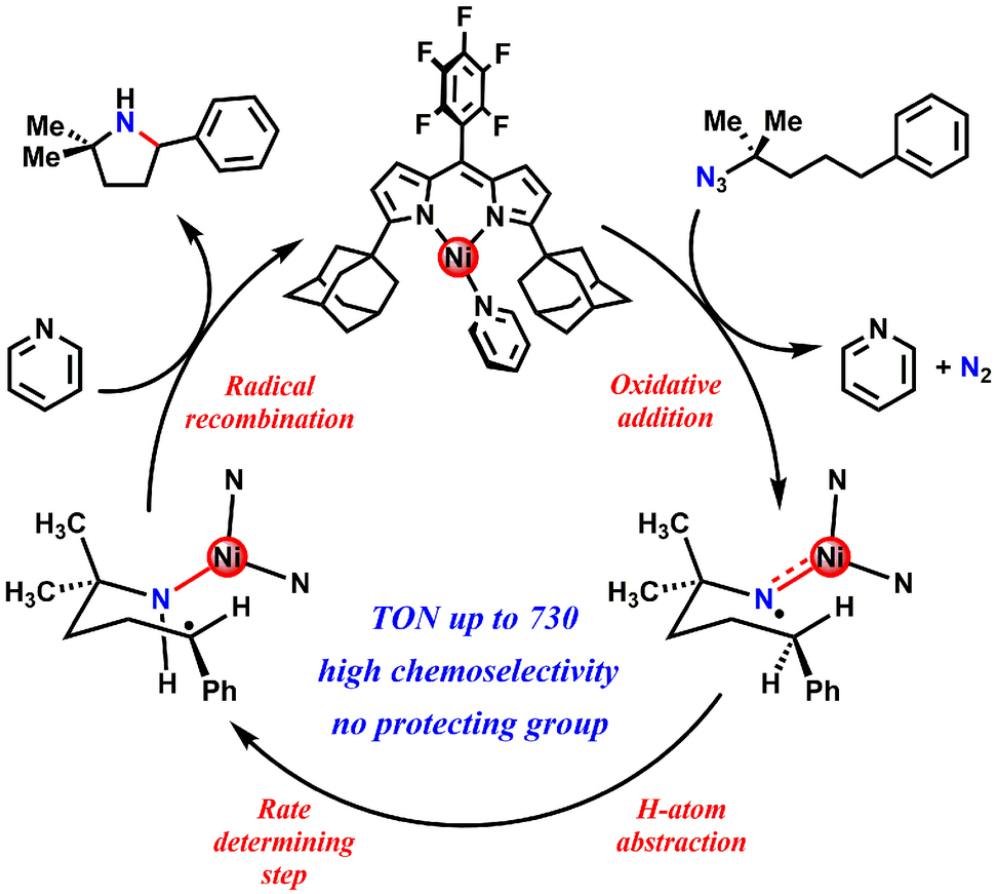

82x74mm (300 x 300 DPI)

Efficient C–H Amination Catalysis Using Nickel-Dipyrrin Complexes

Yuyang Dong, Ryan M. Clarke, Gerard J. Porter and Theodore A. Betley

Department of Chemistry and Chemical Biology, Harvard University, 12 Oxford Street, Cambridge, Massachusetts 02138, United States

KEYWORDS (Word Style "BG_Keywords"). If you are submitting your paper to a journal that requires keywords, provide

ABSTRACT: A dipyrrin-supported nickel catalyst (^{AdF}L)Ni(py) (^{AdF}L: 1,9-di(1-adamantyl)-5-perfluorophenyldipyrrin; py: pyridine) displays productive intramolecular C–H bond amination to afford *N*–heterocyclic products using aliphatic azide substrates. The catalytic amination conditions are mild, requiring 0.1–2% catalyst loading and operational at room temperature. The scope of C–H bond substrates was explored and benzylic, tertiary, secondary, and primary C–H bonds are successfully aminated. The amination chemoselectivity was examined using substrates featuring multiple activatable C–H bonds. Uniformly, the catalyst showcases high chemoselectivity favoring C–H bonds with lower bond dissociation energy as well as a wide range of functional group tolerance (e.g., ethers, halides, thioetheres, esters, etc.). Sequential cyclization of substrates with ester groups could be achieved, providing facile preparation of indolizidine framework that is commonly found in a variety of alkaloids. The amination cyclization reaction mechanism was examined employing nuclear magnetic resonance (NMR) spectroscopy to determine the reaction kinetic profile. A large, primary intermolecular kinetic isotope effect (KIE = 31.9 ± 1.0) suggests H–atom abstraction (HAA) is the rate determining step, indicative of H–atom tunneling being operative. The reaction rate has first order dependence in the catalyst and zeroth order in substrate, consistent with the resting state of the catalyst as the corresponding nickel iminyl radical. The presence of the nickel iminyl was determined by multi-nuclear NMR spectroscopy observed during catalysis. The activation parameters ($\Delta H^{\neq}$ = 13.4 ± 0.5 kcal/mol; $\Delta S^{\neq}$ = –24.3 ± 1.7 cal/mol·K) were measured using Eyring analysis, implying a highly ordered transition state during the HAA step. The proposed mechanism of rapid iminyl formation, rate-determining HAA, and subsequent radical recombination was corroborated by intramolecular isotope labelling experiments and theoretical calculations.

1. INTRODUCTION

Saturated N-heterocycles constitute a critically important class of molecules found in bioactive alkaloids,[1] pharmaceutical agents,[2-3] and as chiral elements in asymmetric catalysis.[4] Indeed, over half of the top twenty best-selling drugs contain an N-heterocycle in the last six years.[2, 5] Cyclic amine architectures form heterocyclic cores in medicines used to treat dementia (solanidine),[5] gastrointestinal dysmotility (SC-53116),[6] mantle cell lymphoma (acalabrutinib),[7] and hepatitis C.[8] Given the ubiquity and importance of N-heterocycles in medicine, streamlined syntheses for these architectures is a high priority.

Traditional strategies to synthesize N-heterocyclic cores include functional group exchange via nucleophilic substitution, rearrangements, cycloadditions, and reductive amination.[9] However, the utility of forming heterocyclic skeletons via direct C–H bond functionalization is becoming a more prevalent strategy. In general, the introduction of diverse chemical functionality into unactivated C–H bonds is an evolving, but not yet solved problem in synthetic chemistry.[10-17] Rendering aliphatic C–H bonds into an interchangeable functional group would greatly expand methodology. Indeed, streamlined syntheses for functionalized products while minimizing waste generation would have tremendous impact on the synthesis of fine chemicals and pharmaceuticals. For examples, over 84% of pharmaceuticals feature at least one N atom,[18] and nearly one in six reactions involve formation of C–N bonds.[19] Thus, direct C–H bond amination methods could provide a streamlined protocol and may serve to enhance the scope of conventional syntheses.

The current state of the art in pyrrolidine synthesis via C–H bond amination largely depend on late transition metal catalysts that template the C–H bond activation followed by a C–N bond forming step.[20-22] Previously, we reported the synthesis of N-heterocycles using an iron catalyzed, intramolecular amination of unactivated aliphatic C–H bonds.[23] The dipyrrin-iron catalyst served to extrude dinitrogen from the azide substrate, leaving an activated iminyl radical[24-26] that could functionalize intramolecular C–H bonds (benzylic, allylic, tertiary, secondary, primary) leading to the formation of cyclic amines. Several limitations with the methodology using dipyrrin-supported iron catalysts included high catalyst loadings and the requirement for product sequestration by *in situ* protection of the secondary amine products.[23, 27] Several groups have adapted this protocol using different catalyst systems, including iron/cobalt porphyrins,[28-30] cobalt corroles,[31] iron bound within redox-active pincer ligands,[32] and iron beta-diketiminate metal

organic frameworks[33] (Figure 1). Each of these systems have improved upon the catalyst performance with regards to decreasing catalyst loading, yet each require elevated reaction temperatures and product sequestration to retard product inhibition. Aryl azide substrates which give rise to cyclic aniline products (far less potent Lewis bases) have been synthesized that bypass this requirement.[34-36] More recently, non-base-metal catalyzed variants have been discovered that employ dirhodium catalysts to effect the amination of aliphatic bonds to generate free amine products following deprotection.[37] While this strategy exhibits remarkable diastereoselectivity, the Rh_2-nitrenoid proposed cannot access primary C–H bond substrates that the high-spin iron catalyzed[23] system can,albeit poorly. Collectively, these strategies highlight how direct, ring-closing amination can generate heterocyclic cores without requiring activating groups[11, 38] and demonstrating modest functional group tolerance compared with cross-coupling protocols.[18, 39-42] Despite these advances, improvements on the state of the art catalysis known include enhancing catalytic performance, increasing functional group tolerance, and an understanding of how different electronic structures give rise to different catalytic capabilities.[12]

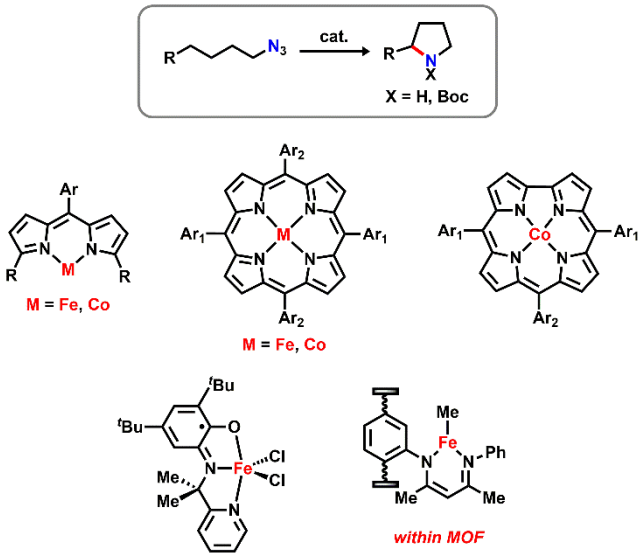

Figure 1. Pyrrolidine synthesis via cyclization C–H amination via base metal catalysts.

Recently we reported that nickel dipyrrinato complexes are capable of stabilizing reactive iminyl functionalities potent for intermolecular functionalization of benzylic C–H bonds.[43] Preparation and characterization of the reactive intermediate suggest an iminyl (^{2}NAr coupled to a triple Ni^{II})or imido (^{1}NR, Ni^{III}) electronic configuration, depending on the N-functional group giving rise to the doublet spin configurations observed. Reaction of the Ni^I complex with 4-(azidobutyl)benzene exclusively formed 4-phenylbutanenitrile (Scheme 1). We report herein that alkylation of the azide-bearing methylene unit mitigates nitrile formation, yielding the corresponding *N*-heterocyclic products. Furthermore, we find the nickel dipyrrin catalyst is effective for amination of benzylic, tertiary, secondary, and primary C–H bonds with high turn-over numbers, mild reaction conditions, and excellent chemoselectivity. A detailed mechanistic study is presented resulting from NMR kinetic profiling of the reaction, corroborated with intramolecular isotope labelling experiments and density functional theory (DFT) computations.

2. RESULTS AND DISCUSSION

Scheme 1.

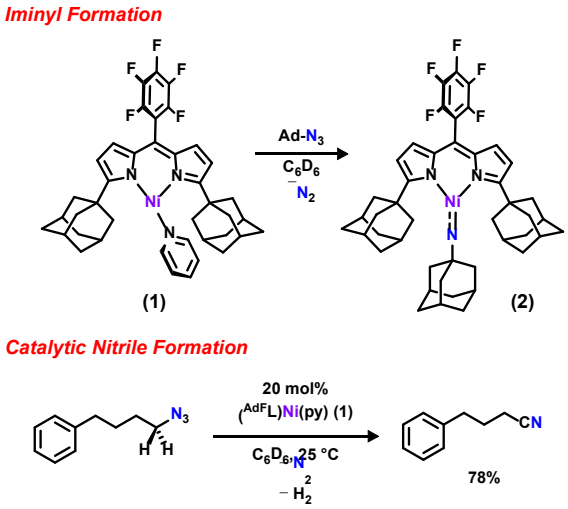

2.1. Catalytic intramolecular C–H amination optimization. In our previous study, (^{AdF}L)Ni(py) (**1**) rapidly consumes tertiary azides to afford the corresponding iminyl complexes (e.g., (^{AdF}L)Ni(NAd) (**2**)) and rapidly converts 4-(azidobutyl)benzene to 4-phenylbutanenitrile via *β*-hydride elimination (Scheme 1). To inhibit nitrile generation, *gem*-dimethyl groups were introduced to the azide substrate to promote C–H bond amination. As an initial test, 10 mol% of (^{AdF}L)Ni(py) (**1**) was subjected to (4-azido-4-methylpentyl)benzene (**3**) in C_6D_6 (Table 1, entry 1). An immediate color change from dark brown to deep pink was observed along with intense effervescence. The ^{19}F NMR spectra obtained during the reaction has similar features to that of **2** (Supplementary Information, Figure S5). Bubbling ceased within 10 min with the solution color reverted to dark brown. Both ^{1}H and ^{19}F NMR spectra of the reaction mixture showed complete regeneration of **1** as well as quantitative conversion of **3** into 2,2-dimethyl-5-phenylpyrrolidine (**4**).

Given the full regeneration of **1**, the catalyst loading was further lowered to 1 mol % without a significant loss in yield (96%). When 0.1 mol% catalyst loading was used, the reaction took two days at room temperature until no further product formation was observed, providing a final NMR yield of 73% (Table 1, entry 1-5; TON_{max} = 730). To compare to dipyrrin iron and cobalt systems, the observed reaction rate of 1.4 min^{-1} (25° C) for **1** is superior to the (^{Ad}L)FeCl[23] and (^{Ar}L)Co(py)[44] systems (require heating > 50 °C) or (^{Tr}L)Co (0.063 min^{-1}),[45] indicating **1** has a much lower activation barrier. The performance and rate of catalysis do not vary significantly with solvent polarity, e.g. from hexanes to THF (Table 1, entry 6-9). Tetrahydrofuran is a catalyst inhibitor for related iron-dipyrrin amination catalysts.[23]

Table 1. Optimization of Amination Conditions[a]

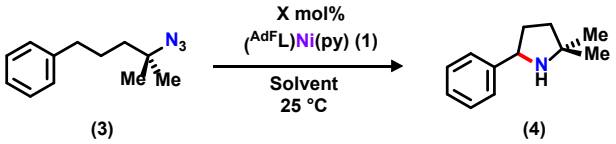

(3) (4)

Entry	Catalyst Loading (mol%)	Solvent	Time	Yield (%)[d]
1	10[b]	C_6D_6	10 min	> 99
2	5[b]	C_6D_6	20 min	> 99
3	2[b]	C_6D_6	40 min	97
4	1[b]	C_6D_6	90 min	96
5	0.1	C_6D_6	48 h	73
6	1[b]	Hexanes	90 min	95
7	1[b]	Et_2O	90 min	96
8	1[b]	(d^8-)Toluene[e]	90 min	95
9	1[b]	d^8-THF	90 min	94
10	10	d^6-DMSO	N/A[c]	0
11	10	d^4-Methanol	N/A[c]	0
12	10	DCM	N/A	0

[a]Reaction were conducted on 0.2 mmol scale, see SI for details of the experiments. [b]Regeneration of **1** by ^{19}F NMR spectroscopy. [c]Catalyst decomposition. [d]Yields were determined by ^1H NMR spectroscopy using tetrakis(trimethylsilyl)silane as internal standard. [e]Both proteo- and deutero-toluene were tested as solvent, and no difference was observed.

Notably, even though the iminyl complex (^{AdF}L)Ni(NAd) (**2**) can abstract the benzylic hydrogen from toluene,[43] the intramolecular reaction is sufficiently faster than intermolecular C–H bond amination that the cyclization reaction can be run in toluene (Table 1, entry 8) without diminishing the yield (95%). However, rapid catalyst decomposition via demetallation was observed in protic (MeOH) and redox-active (DMSO) solvents (Table 1, entry 10-11). We note that the acidic α-H or the trace amount of H_2O in DMSO could also be detrimental to the catalyst performance. When dichloromethane is used as solvent, **1** undergoes instantaneous halogen abstraction, generating the corresponding divalent nickel chloride complex (^{AdF}L)NiCl based on the ^{19}F NMR features of the mixture (Table 1, entry 12).[43] Based on these results, the optimal conditions were chosen to be 1 mol% catalyst loading in C_6D_6 for the ease of reaction monitoring.

2.2. The bond dissociation energy limit of activatable C–H bonds. To test the bond strength limit for activatable C–H bonds of this cyclization reaction, a range of substrates with C–H bonds of various bond dissociation energies was examined (Table 2). Substrate **5** features a primary benzylic C–H bond (BDE: 89.7 ± 1.2 kcal/mol)[46] requires 9 h at room temperature with 10 mol% catalyst loading to be fully converted to the corresponding pyrrolidine product **6**. The same reaction can be completed in only 2 h with 1 mol% catalyst loading heated to 60 °C (65 %). Isolation of the pyrrolidine product **6** was achieved either by an acid-base aqueous extraction or via *N*-tolsylation (addition TsCl, NEt_3, 40 °C, 2 h) followed by column chromatography. Worth noting, the rate difference is likely caused by a combination of an entropically unfavored transition state due to the incorporation of a rigid phenyl group as well as the increased C–H bond dissociation energy in **5** (as compared to **3**).

Substrates with tertiary and secondary aliphatic C–H bonds can also be readily functionalized in good yields using 1 mol% catalyst loading at 60 °C in 6 and 24 h, respectively (**7** and **9**). A higher catalyst loading of 10 mol% was required to aminate a substrate featuring a primary C–H bond (**11**) even at elevated temperature (80 °C, 48 h). Due to the volatility of the product, **12** is separated as an ammonium chloride salt by vacuum transferring into an HCl-diethyl ether solution, leading to a final isolated yield of 35%. Overall, the activable C–H bond strength can be viewed as a proxy for the radical nature of the NR fragment. While the Ni^{II} iminyl system reported herein can activate strong aliphatic C–H bonds, similar catalytic performance was observed with previously reported Fe^{III} iminyl radical species[23, 25] or geometrically constrained Co^{III} imido complexes,[45] showcasing the resemblance of their electronic structures despite different metal oxidation states.

2.3. Chemoselectivity between C–H bonds with different bond dissociation energies. To evaluate the chemoselectivity of this cyclization reaction, azide substrates featuring C–H bonds with different bond dissociation energies were examined under the optimized conditions (entry 1-4; Table 3). Gratifyingly, high levels of chemoselectivity (*d.r.* > 99:1) favoring C–H bonds with lower bond dissociation energies were observed in every substrate tested. Product corresponding to the stronger C–H bonds was undetectable by ^1H NMR spectroscopy. Moreover, when different C–H bonds with similar bond dissociation energy were present in the same substrate in a 2:1 ratio, the expected statistical product mixture (2:1) was obtained (**22a-b**).

2.4. Functional group tolerance. The catalytic amination cyclization reaction tolerates a wide range of functional groups (Table 4): electron rich groups such as thiophene (**23**), furan (**24**), N-methylindole (**25**), phenoxides (**26**-**27**) and thioether (**28**); as well as electron withdrawing groups like aryl halides (**29**-**30**), ester (**31**), and trifluoro methyl groups (**32**). Notably, when the ester group is positioned appropriately, tandem cyclization can be accomplished, leading to indolizidine (**31**) framework that is commonly found in a variety of alkaloids.[47] Substrates with coordinating functional groups such as benzo[d]thiazole (**33**) readily undergoes cyclization in good isolated yield (80%). To examine if large, aromatic substituents alpha to the aminated C–H bond would impede catalysis, a pyrene terminated substrate (**34**) was examined and did not impact catalysis.

An aliphatic azide featuring a pendant alkyl bromide (**35**) leads to rapid catalyst decomposition in a similar way that dichloromethane deactivates the catalyst via Cl-atom abstraction (Table 1, entry 12). Acidic functional groups such as phenol (**36**) also leads to rapid catalyst decomposition likely via proto-demetallation (free (^{AdF}L)H observed by ^1H

Table 2. Substrates with various bond dissociation energies[a]

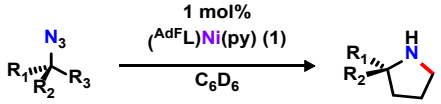

Entry	Substrate	Time (h)	Temperature (°C)	Product	Yield (%)[a]
1	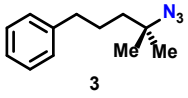 3	2	25	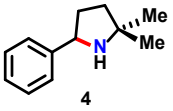 4	95
2	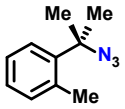 5	9[b]/2	25[b]/60	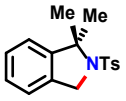 6[c]	65
3	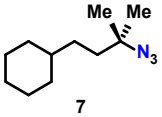 7	6	60	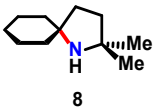 8	88
4	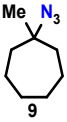 9	24	60	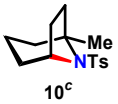 10[c]	72
5	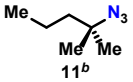 11[b]	48	80	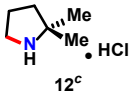 12[c]	35

[a]Isolated yields; [b]10 mol% of ([AdF]L)Ni(py) (**1**) was used; [c]Derivatized for ease of isolation. Combined yield for two steps.[48]

Table 3. Substrates with competitive C–H bonds of different bond dissociation energies[a]

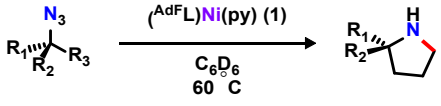

Entry	Substrate	Time (h)	Product	Yield (%)[b]
1	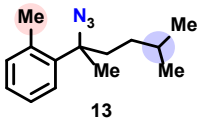 13	4	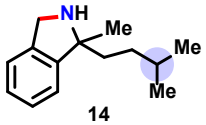 14	71
2	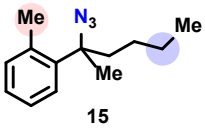 15	4	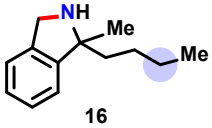 16	65
3	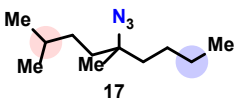 17	6	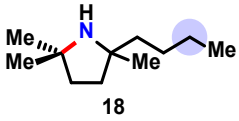 18	82

4	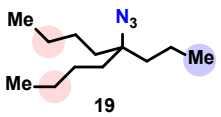 **19**	24	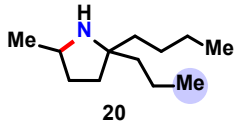 **20**	85
5	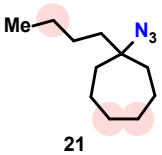 **21**	24	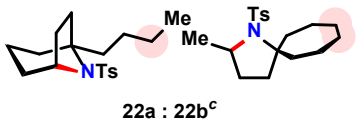 **22a : 22b**[c] **2 : 1**	67

[a]Within each substrate, the more activated C–H bonds are noted with red circles, and the less activated ones are labeled with blue circles; [b]Isolated yields; [c]Derivatized for ease of isolation. Combined yield for two steps.[48]

Table 4. Functional group tolerance[a]

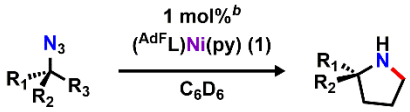

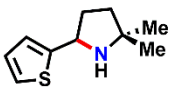 **23** 2 mol%, 25 °C, 2 hrs 92 %	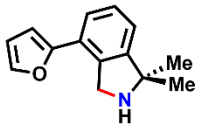 **24** 2 mol%, 60 °C, 2 hrs 84 %	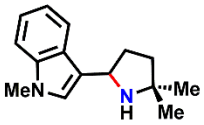 **25** 25 °C, 2 hrs 91 %	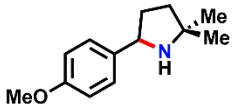 **26** 25 °C, 2 hrs 82 %	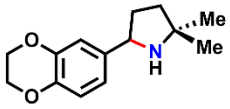 **27** 2 mol%, 60 °C, 2 hrs 75 %
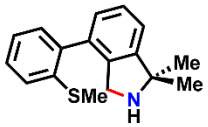 **28** 2 mol%, 60 °C, 2 hrs 65 %	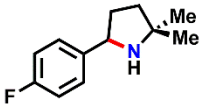 **29** 25 °C, 2 hrs 94 %	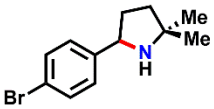 **30** 25 °C, 2 hrs 82 %	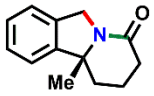 **31** 1) 60 °C, 2 hrs 2) K_2CO_3, MeOH, 10 hrs 66 %	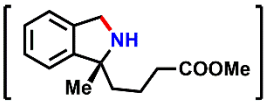
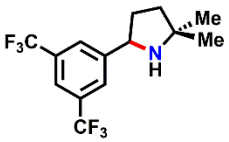 **32** 25 °C, 2 hrs 80 %	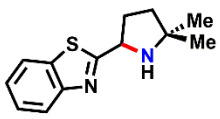 **33** 25 °C, 2 hrs 80 %	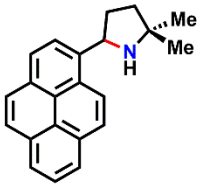 **34** 25 °C, 2 hrs 77 %	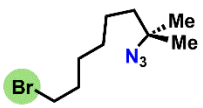 **35**[c] 10 mol%, 80 °C, 24 hrs no reaction	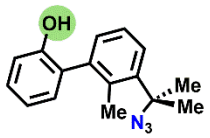 **36**[c] 10 mol%, 80 °C, 24 hrs no reaction
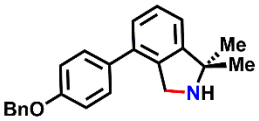 **37** 2 mol%, 60 °C, 2 hrs 76 %	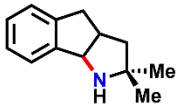 **38** syn:anti > 99:1 25 °C, 2 hrs 73 %	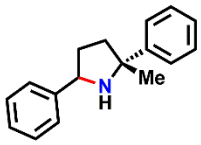 **39** d.r. = 4.3 : 1 25 °C, 4 hrs 89 %	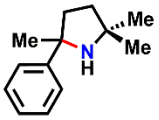 **40** 25 °C, 2 hrs 84 %	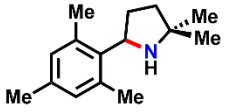 **41** 10 mol%, 80 °C, 24 hrs trace

[a]All yields noted are isolated yields; [b]Default catalyst loading (1 mol %) unless noted otherwise; [c]functional groups detrimental to the catalysis are highlighted in green.

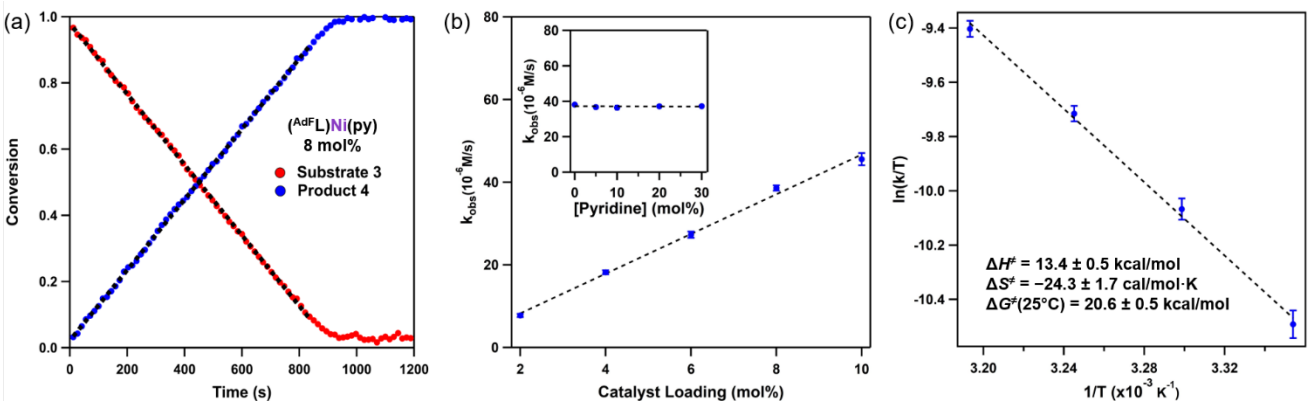

Figure 2. (a) Conversion of substrate **3** into **4** as a function of time using 8 mol% of **1**. The black dashed line represents the linear fit over the first three half-lives ($3\tau_{1/2}$) used to extracted k_{obs} values. (b) Observed rate constants as a function of catalyst loadings with every measurement done in triplicate. Error bars represent standard deviations. Inset: observed rate constants as a function of exogenous pyridine concentrations using 8 mol% of **1**. Every measurement is done in triplicate, and error bars represent standard deviations. (c) Eyring analysis with every measurement done in triplicate. Error bars represent standard deviations. Parameters extracted from the Eyring plot: $\Delta H^{\neq}$ = 13.4 ± 0.5 kcal/mol; $\Delta S^{\neq}$ = −24.3 ± 1.7 cal/mol·K; $\Delta G^{\neq}$(25°C) = 20.6 ± 0.5 kcal/mol.

NMR spectroscopy). However, substrates containing protected phenol such as benzyloxy group can be readily cyclized (**37**).

When the cyclization leads to a fused ring structure (**38**), high level of diastereoselectivity is observed (*syn*:*anti* > 99:1).[49] The minor *anti* isomer is not detectable by ^{1}H NMR spectroscopy. If different α-methylene substituents are introduced at the *gem* position (Ph/Me), the reaction exhibits a moderate level of diastereoselectivity (**39**, *d.r.* = 4.3:1; 83%).[27] Although the pyrene substituent in **34** and sterically encumbered tertiary benzylic C–H bond (**40**) undergo cyclization smoothly, the mesityl substituent in **41** only led to trace amounts of the cyclized product, likely owing to the *ortho*-phenyl substituents that can sterically impede activation.

2.5. Mechanistic study. To elucidate the mechanism of the amination cyclization, the concentrations of azide **3** and product **4** during the catalytic reaction with 8 mol% of **1** at room temperature were measured as a function of time (Figure 2a) using ^{1}H NMR spectroscopy. Linear relationships were observed for product generation and azide consumption over time ($3\tau_{1/2}$, 14 min), indicating a zeroth order dependence of the reaction rate on the substrate concentration. Similar experiments were carried out using various catalyst loadings from 2–10 mol%. Plotting the slopes obtained from first three half-lives of each run (k_{obs}) versus catalyst loadings reveals a linear relationship, indicating a first order dependence of the reaction rate on the catalyst loading (Figure 2b). Each kinetic experiment is reproduced in triplicate, and error bars are plotted using the standard deviations. The ^{1}H and ^{19}F NMR spectra during catalysis indicate complete conversion of **1** into a paramagnetic species with similar spectroscopic features to the previously reported (^{AdF}L)Ni(NAd) (**2**) (Figure S5). Notably, the concentration of the new species remains constant over the course of the reaction, suggesting the resting state of the catalyst is the corresponding nickel(II) iminyl species. Complete regeneration of catalyst (^{AdF}L)Ni(py) (**1**) was observed after reaction completion by ^{19}F NMR spectroscopy.

Considering our recently reported cobalt dipyrrin catalytic system whose rate depends on concentration of exogenous L-type ligand such as pyridine,[44] we sought to examine if a similar effect exists for the nickel system. As the isolated nickel adamantyl iminyl complex **2** does not have pyridine bound, several catalytic runs with 8 mol% catalyst loading were carried out with pyridine ranging from 0–30 mol% added. Based on the k_{obs} values extracted from the slopes over first three half-lives of the trial runs, the reaction rate does not vary significantly with exogenous pyridine concentrations (Figure 2b), possibly due to the increased electronegativity of nickel compared to cobalt.[44-45] Notably, at high pyridine concentration (30 mol%), even though the product generation follows a linear relationship over the first three half-lives, the correlation deviates from linearity at low substrate concentration, indicating a competitive binding equilibrium between the substrate **3** and pyridine.

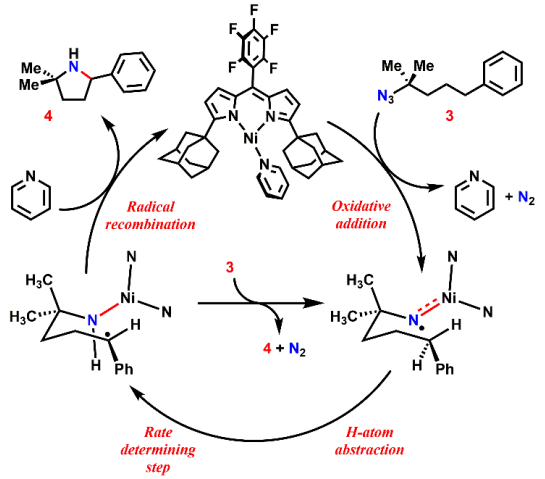

Figure 3. Proposed mechanism for C–H amination.

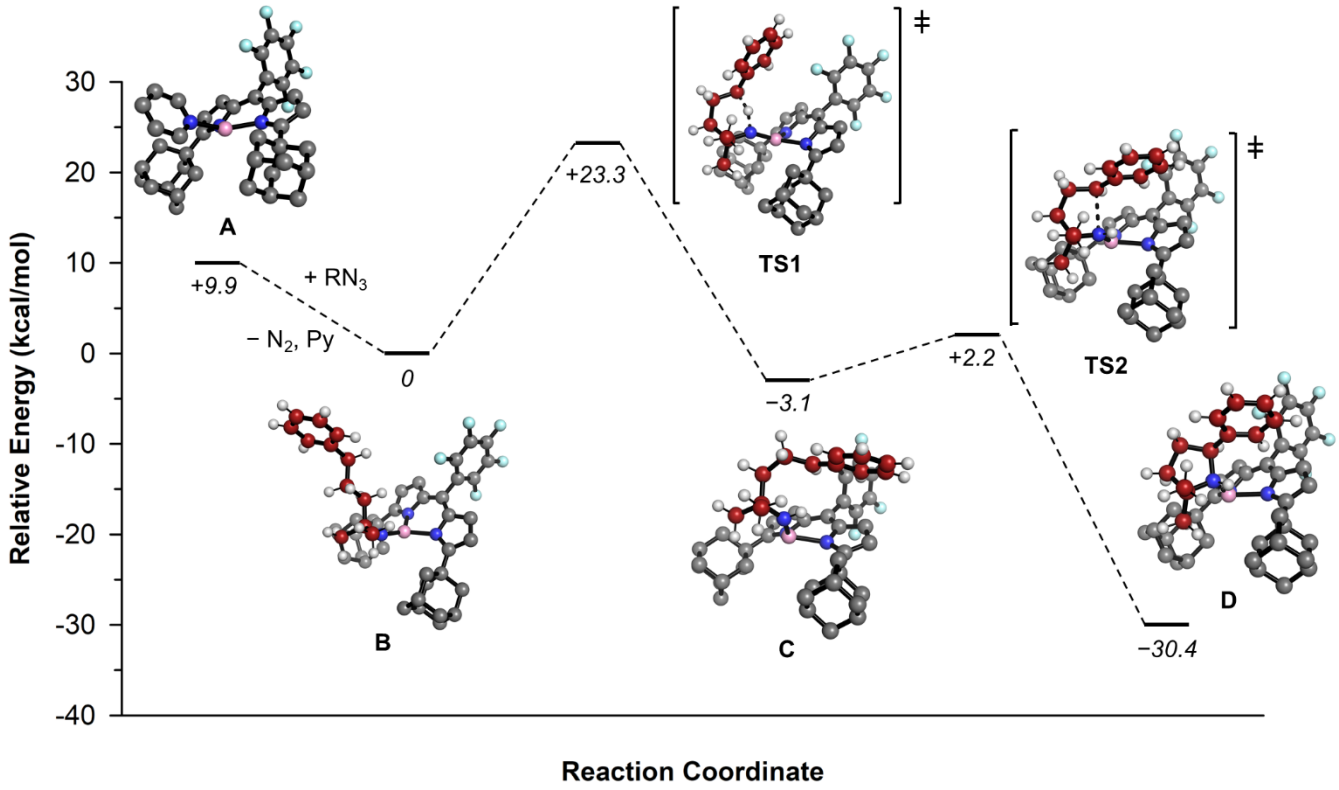

Figure 4. DFT calculated reaction pathway for the cyclization of **3** into 2-phenyl-5,5-dimethylpyrrolidine (**4**) mediated by (^{AdF}L)Ni(py) (**1**). Energies are reported in kcal/mol relative to the (^{AdF}L)Ni($^{\bullet}$NR) catalyst resting state. [B3LYP/ def2-SVP (C, H) and def2-TZVP (Ni, N, F)][50-53]

We have shown in our previous Fe- and Co-based catalytic systems by measuring the kinetic isotope effects that H-atom abstraction contributes to the rate determining step of the amination.[23, 27, 44-45] Similarly, the bis-deutero substituted substrate (4-azido-4-methylpentyl-1,1-d_2)benzene (**3**$_{D2}$) was prepared and treated with 8 mol% of **1**. By measuring concentration of the product **4**$_D$ over time (Figure S**4**), an intermolecular kinetic isotope effect of 31.9 ± 1.0 was determined. The large KIE value indicates the C–H bond activation features prominently in the rate determining step and, furthermore, either goes through a radical-based, H atom abstraction with significant tunneling or can indicate a highly linear transition state between the H-atom donor and acceptor. [42] Given the configurational restriction by tunneling effect, a large, negative activation entropy is expected. Indeed, by conducting the same kinetic experiment at various temperatures and performing Eyring analysis, activation enthalpy of 13.4 ± 0.5 kcal/mol and activation entropy of −24.3 ± 1.7 cal/mol·K were obtained, consistent with other previously reported kinetic measurements on similar 1,5-HAA reactions (Figure 2c).[54-55]

Based on the above kinetic measurements, a catalytic cycle is proposed (Figure 3). Substrate **3** displaces pyridine from **1**, followed by release of dinitrogen giving rise to the corresponding nickel iminyl species (e.g., $Ni^{II}(^2NR)$) as the resting state of the catalyst.[43] The next step is the rate-determining hydrogen atom abstraction via tunneling followed by radical recombination to furnish the bound cyclized product. Product displacement is aided by ligand substitution with pyridine or substrate **3**, releasing the pyrrolidine product **4**. Since **3** enters the cycle before the resting state, the reaction rate is not dependent on its concentration.[42]

2.6. Theoretical Modelling of the Reaction Profile. Density functional theory (DFT) calculations were employed in order to provide support for the proposed mechanism in Figure 4, and to gain insight into geometric factors that may influence substrate turnover during catalysis. The calculations were performed with the B3LYP functional and the def2-SVP (C, H) and def2-TZVP (Ni, N, F) basis sets on an untruncated system.[50-53] The full computational methodology is described in detail in the Supporting Information. We first optimized the minima along the reaction coordinate corresponding to the resting state alkyl iminyl species **B** and the ring-closed, pyrrolidine bound **D**. The DFT optimized resting state **B** has similar coordination bond lengths (Ni–N_{im} = 1.668 Å) to the crystallographically characterized adamantyl imido we previously described (Ni–N_{im} = 1.642(7) Å), whereas the product bound **D** has a significantly longer Ni–N_{im} bond, (Ni–N_{im} = 2.126 Å) more in line with the Ni(I) catalyst (**1**) (Ni–N_{pyr} = 1.9566(19) Å). Product-bound **D** is 30.4 kcal/mol lower in energy relative to the catalyst resting state. In order to locate transition states corresponding to hydrogen-atom abstraction (HAA – **TS1**) and pyrrolidine ring closure (**TS2**) as a result of alkyl radical rebound, a relaxed potential energy surface scan along the C_4–

N_{im} bond vector (20×0.1 Å steps) was conducted starting from the product bound **D** and searching for an energy maximum. The corresponding maximum energy geometry was then subjected to a transition state optimization, resulting in a species with a single imaginary frequency (ν_{im} = −297 cm^{-1}) located 32.6 kcal/mol above the ring closed product, corresponding to **TS2**, ring closure between C_4 and N_{im} as a result of alkyl radical rebound. Connectivity between **TS2** and **D** was established via an intrinsic reaction coordinate (IRC) calculation, during which the Ni–N_{im} bond length lengthens substantially (1.877 Å in **TS2** to 2.126 Å in **D**) while moving along the reaction coordinate. Furthermore, C_4 is planarized in **TS2**, suggesting radical character at that position.

We then endeavored to locate the transition state corresponding to H–atom abstraction by moving the proton from N_{im} back to C_4 and performing an optimization, resulting in a local minimum immediately preceding HAA (see the suppsupporting Information for geometry and coordinates, Figure S13–S19, Table S2–S8). A relaxed potential energy surface scan along the N_{im}–H vector located a maximum energy structure which was optimized to a transition state corresponding to HAA with a single imaginary frequency (ν_{im} = −1693 cm^{-1}) located 23.3 kcal/mol above the catalyst resting state. While this is in excellent agreement with the barrier determined experimentally (20.6 ± 0.5 kcal/mol), the intermediate **C** following HAA and preceding radical rebound was found as confirmation of HAA as rate determining. The reaction coordinate was followed in the forward direction from **TS1** to locate a local minimum structure preceding radical rebound, located 5.3 kcal/mol below **TS2**. This modest barrier to radical rebound agrees with HAA as the rate determining step by both experimental and theoretical means.

2.7. Intramolecular isotope labelling experiment. In order to gain kinetic information on the rate of radical recombination step, a pair of isotopically labelled enantiopure substrates (**S-3$_{HD}$** and **R-3$_{HD}$**) were prepared.[56] Subjecting this pair of substrates to standard catalytic conditions could lead to four potential products: **S-4$_H$**, **R-4$_H$**, **S-4$_D$** and **R-4$_D$** (**S-3$_{HD}$**: Figure 5; **S-3$_{HD}$** and **R-3$_{HD}$**: Figure S7). The two pairs of enantiomers (**S-4$_H$**, **R-4$_H$**; **S-4$_D$**, **R-4$_D$**) are resolved using Mosher analysis[57-58] by condensing the isolated mixture of **4$_H$** and **4$_D$** with (*S*)-(+)-α-Methoxy-α-(trifluoromethyl)phenylacetyl chloride (S-Mosher acyl chloride). The product distributions are obtained from ^{1}H NMR spectrum of the final mixture. Since catalyst **1** is achiral and the pair of substrates (**S-3$_{HD}$** and **R-3$_{HD}$**) are enantiomers, the same product distribution with inverted chirality should be expected from both reactions. Indeed, the same distribution was observed with a large ratio between **4$_D$** and **4$_H$** in both cases, suggesting the H–atom abstraction is favored over its deuterium counterpart, yielding an intramolecular KIE of 18.1 greater than related iron and cobalt dipyrrin systems,[23, 44] but less than the geometrically restricted Co-based catalyst.[45]

Once the H/D-atom is abstracted, two processes take place in competition: the planar, carbon-based benzyl radical rotation to expose either the *Re* or *Si* face near the iminyl N, and radical rebound to form the C–N bond. Given the substrates **S-3$_{HD}$** and **R-3$_{HD}$** are enantiopure, if the rate of radical trapping process exceeds that of the carboradical rotation, the corresponding enantiopure pyrrolidines (**4$_H$** or **4$_D$**) should be expected. Otherwise, if the radical rebound process is sufficiently slow that the carboradical rotation reaches thermo-equilibrium first, completely racemic mixtures would be observed instead. The experimental results, however, revealed an intermediate ratio of 4.6 (average from two reactions) between the major and minor isomers. The intermediate value suggests that radical is trapped before its rotation could reach thermo-equilibrium, suggesting that the two processes happen on a comparable time scale. A similar strategy to probe the rate of radical rebound has been used to examine the mechanism of C–H hydroxylation using cytochrome P450,[59] intramolecular C–H insertion using iron-carbene complexes,[60] allylic C–H abstraction by singlet oxygen,[61] and more recently enantioselective carbene C–H insertion catalyzed by chiral cobalt porphyrin complexes.[62] In relation to our previously published dipyrrinato Fe system[23] with a smaller KIE of 5.3 and Co catalyst that only exhibits a large KIE of 38.4(1) upon geometry distortion of the imido fragment to resemble the HAA transition state,[45] we hypothesize that the linear approach of the C–H bond toward to iminyl N-atom would result in the corresponding amide H-atom blocking the effective radical recombination pathway, allowing the alkyl radical rotation to happen prior to intramolecular capture.

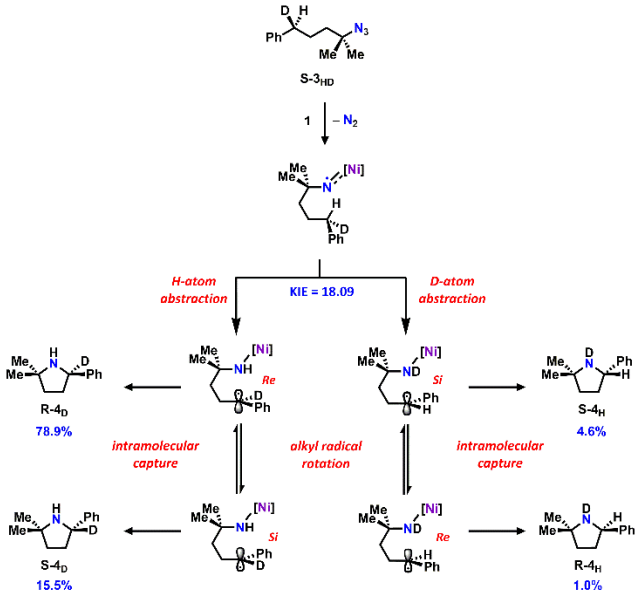

Figure 5. Product distribution using enantiopure mono D-labeled substrates **S-3$_{HD}$**, The two pairs of enantiomers (**S-4$_H$** and **R-4$_H$**; **S-4$_D$** and **R-4$_D$**) are resolved using Mosher analysis[57-58] and the ratios are obtained using ^{1}H NMR spectroscopy. All reactions were carried out using standard catalytic conditions at room temperature (25 °C).

Based on these results, two potential strategies toward enantioselective C–H amination catalysis can be proposed depending on the relative rate between radical recombination and rotation.[62] If the radical rebound is much faster, the enantioselectivity is solely determined by the H–atom

abstraction step. Therefore, the catalyst should have its chiral elements proximal to the iminyl nitrogen. If, however, carboradical rotation reaches thermo-equilibrium first, the reaction will be under Curtin-Hammett control.[42, 62] The enantioselectivity is then dictated by the relative barrier height of the radical rebound process with *Re* or *Si* face of the carbon-based radical. In this case, the catalyst should be designed to better accommodate one prochiral face of the radical versus the other. The enantioselective C–H amination catalysis is currently under study.

3. CONCLUSION

In conclusion, we have developed an efficient nickel dipyrrinato catalyst capable of aminating strong, aliphatic C–H bonds with simple ligand synthesis, low catalyst loading, mild reaction conditions, wide substrate scope and high chemoselectivity. From an electronic structure standpoint, the reactive intermediate proposed in the Ni-based catalytic cycle is a Ni^{II} iminyl radical,[43] akin to those encountered in the Fe^{II} dipyrrin-supported catalysts.[23-26] Catalysts that either accumulate radical character on the nitrenoid fragment[23-26] or geometrically predispose the reactive intermediate to being reactive[45] are more potent oxidants than related systems that traverse through imido-like intermediates.[44] A detailed mechanistic study was also carried out to provide insights into further improvements of the Ni catalyst. Theoretical studies closely reproduced experimentally measured kinetics barriers, corroborating the proposed mechanistic cycle. Intramolecular isotope labelling experiment suggests that the radical recombination step happens on the same time scale as the radical rotation. Based on these results, two potential strategies for enantioselective amination are proposed, and catalysts competent for such enantioselective catalysis are currently under study.

ASSOCIATED CONTENT

The Supporting Information is available free of charge on the ACS Publications website.
General experimental considerations and procedures, multinuclear NMR data (PDF)

AUTHOR INFORMATION

Corresponding Author

*betley@chemistry.harvard.edu

Notes

The authors declare no competing financial interest.

ACKNOWLEDGMENT

This work was generously supported by a grant from the NIH (GM-115815), the Dreyfus Foundation (Teacher-Scholar Award to T.A.B.), and Harvard University. R.M.C. gratefully acknowledges an NSERC Postdoctoral Fellowship.

REFERENCES

1. Fattorusso, E.; Taglialatela-Scafati, O., *Modern alkaloids: structure, isolation, synthesis, and biology*. John Wiley & Sons: 2008.
2. Vitaku, E.; Smith, D. T.; Njardarson, J. T. Analysis of the structural diversity, substitution patterns, and frequency of nitrogen heterocycles among U.S. FDA approved pharmaceuticals. *J. Med. Chem.* **2014**, *57*, 10257.
3. Taylor, R. D.; MacCoss, M.; Lawson, A. D. G. Rings in drugs. *J. Med. Chem.* **2014**, *57*, 5845.
4. Banik, S. M.; Levina, A.; Hyde, A. M.; Jacobsen, E. N. Lewis acid enhancement by hydrogen-bond donors for asymmetric catalysis. *Science* **2017**, *358*, 761.
5. Race, N. J.; Hazelden, I. R.; Flaulkner, A.; Bower, J. F. Recent developments in the use of aza-Heck cyclizations for the synthesis of chiral N-heterocycles. *Chem. Sci.* **2017**, *8*, 5248.
6. Flynn, D. L.; Zabrowski, D. L.; Becker, D. P.; Nosal, R.; Villamil, C. I.; Gullikson, G. W.; Moummi, C.; Yang, D. C. SC-53116: the first selective agonist at the newly identified serotonin 5-HT4 receptor subtype. *J. Med. Chem.* **1992**, *35*, 1486.
7. Wang, M.; Rule, S.; Zinzani, P. L.; Goy, A.; Casasnovas, O.; Smith, S. D.; Damaj, G.; Doorduijn, J.; Lamy, T.; Morschhauser, F.; Panizo, C.; Shah, B.; Davies, A.; Eek, R.; Dupuis, J.; Jacobsen, E.; Kater, A. P.; Le Gouill, S.; Oberic, L.; Robak, T.; Covey, T.; Dua, R.; Hamdy, A.; Huang, X.; Izumi, R.; Patel, P.; Rothbaum, W.; Slatter, J. G.; Jurczak, W. Acalabrutinib in relapsed or refratory matle cell lymphoma (ACE-LY-004): a single-arm, multicentre, phase 2 trial. *Lancet* **2018**, *391*, 659.
8. Poordad, F.; Felizarta, F.; Asatryan, A.; Sulkowski, M. S.; Reindollar, R. W.; Landis, C. S.; Gordon, S. C.; Flamm, S. L.; W., F. M.; Bernstein, D. E.; Lin, C. W.; Liu, R.; Lovell, S. S.; I., N. T.; Kort, J.; Mensa, F. J. Glecarprevir and pirbrentasvir for 12 weeks for hepatitis C virus gentype 1 infection and prior direct-acting antiviral treatment. *Hepatology* **2017**, *66*, 389.
9. Candeias, N. R.; Branco, L. C.; Gois, P. M. P.; Afonso, C. A. M.; Trindade, A. F. More sustainable approaches for the synthsis of N-based heterocycles. *Chem. Rev.* **2009**, *109*, 2703.
10. Labinger, J. A.; Bercaw, J. E. Understanding and exploiting C–H bond activation. *Nature* **2002**, *417*, 507.
11. Dick, A. R.; Sanford, M. S. Transition metal catalyzed oxidative functionalization of carbon–hydrogen bonds. *Tetrahedron* **2006**, *62*, 2439.
12. Goswami, M.; Lyaskovskyy, V.; Domingos, S. R.; Buma, W. J.; Woutersen, S.; Troeppner, O.; Ivanović-Burmazović, I.; Lu, H.; Cui, X.; Zhang, X. P.; Reijerse, E. J.; DeBeer, S.; van Schooneveld, M. M.; Pfaff, F. F.; Ray, K.; de Bruin, B. Characterization of porphyrin-Co(III)-'nitrene radical' species relevant in catalytic nitrene transfer reactions. *J. Am. Chem. Soc.* **2015**, *137*, 5468.
13. Li, C.; Lang, K.; Lu, H.; Hu, Y.; Cui, X.; Wojtas, L.; Zhang, X. P. Catalytic radical process for enantioselective amination of C(sp^3)–H bonds. *Angew. Chem. Int. Ed.* **2018**, *57*, 16837.
14. Lu, H.; Hu, Y.; Jiang, H.; Wojtas, L.; Zhang, X. P. Stereoselective radical amination of electron-deficient C(sp^3)–H bonds by Co(II)-based metalloradical catalysis: direct synthesis of α-amino acid derivatives via α-C–H amination. *Org. Lett.* **2012**, *14*, 5158.
15. Lu, H.; Jiang, H.; Hu, Y.; Wojtas, L.; Zhang, X. P. Chemoselective intramolecular allylic C–H amination versus C=C aziridination through Co(ii)-based metalloradical catalysis. *Chem. Sci.* **2011**, *2*, 2361.
16. Lu, H.; Lang, K.; Jiang, H.; Wojtas, L.; Zhang, X. P. Intramolecular 1,5-C(sp^3)–H radical amination via Co(ii)-based metalloradical catalysis for five-membered cyclic sulfamides. *Chem. Sci.* **2016**, *7*, 6934.
17. Lu, H.; Li, C.; Jiang, H.; Lizardi, C. L.; Zhang, X. P. Chemoselective amination of propargylic C(sp^3)–H bonds by cobalt(II)-based metalloradical catalysis. *Angew. Chem. Int. Ed.* **2014**, *53*, 7028.
18. Vitaku, E.; Smith, D. T.; Njardarson, J. T. Analysis of the structural diversity, substitution patterns, and frequency of nitrogen heterocycles among U.S. FDA approved pharmaceuticals. *J. Med. Chem.* **2014**, *57*, 10257.
19. Roughley, S. D.; Jordan, A. M. The medicinal chemist's toolbox: an analysis of reactions used in the pursuit of drug candidates. *J. Med. Chem.* **2011**, *54*, 3451.
20. Nakamura, I.; Yamamoto, Y. Transition-metal-catalyzed reactions in heterocyclic synthesis. *Chem. Rev.* **2004**, *104*, 2127.

21. Gandeepan, P.; Müller, T.; Zell, D.; Cera, G.; Warratz, S.; Ackermann, L. 3d Transition metals for C–H activation. *Chem. Rev.* **2019**, *119*, 2192.
22. Park, Y.; Kim, Y.; Chang, S. Transition metal-catalyzed C–H amination: scope, mechanism, and applications. *Chem. Rev.* **2017**, *117*, 9247.
23. Hennessy, E. T.; Betley, T. A. Complex *N*-Heterocycle synthesis via iron-catalyzed, direct C-H bond amination. *Science* **2013**, *340*, 591.
24. King, E. R.; Hennessy, E. T.; Betley, T. A. Catalytic C-H bond amination from high-spin iron imide complexes. *J. Am. Chem. Soc.* **2011**, *133*, 4917.
25. Wilding, M. J. T.; Iovan, D. A.; Wrobel, A. T.; Luken, J. T.; MacMillan, S. N.; Lancaster, K. M.; Betley, T. A. Direct comparison of C–H bond amination efficacy through manipulation of nitrogen-valance centered redox: imido versus iminyl. *J. Am. Chem. Soc.* **2017**, *139*, 14757.
26. Iovan, D. A.; Betley, T. A. Characterization of iron–imido species relevant for N–group transfer chemistry. *J. Am. Chem. Soc.* **2016**, *138*, 1983.
27. Iovan, D. A.; Wilding, M. J. T.; Baek, Y.; Hennessy, E. T.; Betley, T. A. Diastereoselective C–H bond amination for disubstituted pyrrolidines. *Angew. Chem. Int. Ed.* **2017**, *56*, 15599.
28. Du, Y.-D.; Xu, Z.-J.; Zhou, C.-Y.; Che, C.-M. An effective [Fe^{III}(TF_4DMAP)Cl] catalyst for C-H bond amination with aryl and alkyl azides. *Org. Lett.* **2019**, *21*, 895.
29. Shing, K.-P.; Liu, Y.; Cao, B.; Chang, X.-Y.; You, T.; Che, C.-M. N-heterocyclic carbene iron(III) porphyrin-catalyzed intramolecular C(sp^3)-H amination of alkyl azides. *Angew. Chem. Int. Ed.* **2018**, *57*, 11947.
30. Kuijpers, P. F.; Tiekink, M. J.; Breukelaar, W. B.; Broere, D. L. J.; van Leest, N. P.; van der Vlugt, J. I.; Reek, J. N. H.; de Bruin, B. Cobalt-porphyrin-catalysed intramolecular ring-closing C–H amination of aliphatic azides: a nitrene-radical approach to saturated heterocycles. *Chem. Eur. J.* **2017**, *23*, 7945.
31. Goswami, M.; Geuijen, P.; Reek, J. N. H.; de Bruin, B. Application of [Co(Corrole)]$^-$ complexes in ring-closing C-H amination of aliphatic azides via nitrene radical intermediates. *Eur. J. Inorg. Chem.* **2018**, 617.
32. Bagh, B.; Broere, D. L. J.; Sinha, V.; Kuijpers, P. F.; van Leest, N. P.; de Bruin, B.; Demeshko, S.; Siegler, M. A.; van der Vlugt, J. I. Catalytic synthesis of N-heterocycles via direct C(sp3)–H amination using an air-stable iron(III) species with a redox-active ligand. *J. Am. Chem. Soc.* **2017**, *139*, 5117.
33. Thacker, N. C.; Lin, Z.; Zhang, T.; Gilhula, J. C.; Abney, C. W.; Lin, W. Robust and porous β-diketiminate-functionalized metal–organic frameworks for earth-abundant-metal-catalyzed C–H amination and hydrogenation. *J. Am. Chem. Soc.* **2016**, *138*, 3501.
34. Alt, I. T.; Guttroff, C.; Plietker, B. Iron-catalyzed intramolecular aminations of C(sp^3)-H bonds in alkylaryl azides. *Angew. Chem. Int. Ed.* **2017**, *56*, 10582.
35. Liu, Y.; Wei, J.; Che, C.-M. [Fe(F_{20}TPP)Cl] catalyzed intramolecular C-N bond formation for alkaloid synthesis using aryl azides as nitrogen source. *Chem. Commun.* **2010**, *46*, 6926.
36. Villanueva, O.; Weldy, N. M.; Blakey, S. B.; MacBeth, C. E. Cobalt catalyzed sp^3 C-H amination utilizing aryl azides. *Chem. Sci.* **2015**, *6*, 6672.
37. Munnuri, S.; Adebesin, A. M.; Paudyal, M. P.; Yousufuddin, M.; Dalipe, A.; Falck, J. R. Catalyst-controlled diastereoselective synthesis of cyclic amines via C-H functionalization. *J. Am. Chem. Soc.* **2017**, *139*, 18288.
38. Hinman, A.; Du Bois, J. A stereoselective synthesis of (-)-tetrodotoxin. *J. Am. Chem. Soc.* **2003**, *125*, 11510.
39. Hartwig, J. F., *Organtransition Metal Chemistry: From Bonding to Catalysis*. University Science Books: Mill Valley, CA, 2010.
40. Hartwig, J. F. Catalyst-controlled site-selective bond activation. *Acc. Chem. Res.* **2017**, *50*, 549.
41. Hartwig, J. F. Borylation and silylation of C-H bonds: a platform for diverse C-H bond functionalizations. *Acc. Chem. Res.* **2012**, *45*, 864.
42. Anslyn, E. V.; Dougherty, D. A., *Modern Physical Organic Chemistry*. University Science Books: Sausalito, 2006.
43. Dong, Y.; Lukens, J. T.; Clarke, R. M.; Zheng, S. L.; Lancaster, K. M.; Betley, T. A. Synthesis, characterization and C-H amination reactivity of nickel iminyl complexes. *Chem. Sci.* **2020**, *11*, 1260.
44. Baek, Y.; Betley, T. A. Catalytic C–H Amination Mediated by Dipyrrin Cobalt Imidos. *J. Am. Chem. Soc.* **2019**, *141*, 7797.
45. Baek, Y.; Hennessy, E. T.; Betley, T. A. Direct manipulation of metal imido geometry: key principles to enhance C-H amination efficacy. *J. Am. Chem. Soc.* **2019**, *141*, 16944.
46. Luo, Y.-R., *Comprehensive Handbook of Chemical Bond Energies*. 1st ed.; CRC Press: Boca Raton, 2007.
47. Howard, A. S.; Michael, J. P., Chapter 3. Simple Indolizidine and Quinolizidine Alkaloids. In *The Alkaloids: Chemistry and Pharmacology*, Brossi, A., Ed. Academic Press: San Diego, 1986; Vol. 28, pp 183-308.
48. Wang, X.; Chen, Z.; Sun, X.-L.; Tang, Y.; Xie, Z. Intramolecular hydroamination of aminoalkenes catalyzed by a cationic zirconium complex. *Org. Lett.* **2011**, *13*, 4758.
49. Wang, H.-M.; Zhou, H.; Xu, Q.-S.; Liu, T.-S.; Zhuang, C.-L.; Shen, M.-H.; Xu, H.-D. Copper-catalyzed borylative cyclization of substituted *N*-(2-vinylaryl)benzaldimines. *Org. Lett.* **2018**, *20*, 1777.
50. Schäfer, A.; Horn, H.; Ahlrichs, R. Fully optimized contracted Gaussian basis sets for atoms Li to Kr. *J. Chem. Phys.* **1992**, *97*, 2571.
51. Becke, A. D. Density‐functional thermochemistry. III. The role of exact exchange. *J. Chem. Phys.* **1993**, *98*, 5648.
52. Becke, A. D. A new mixing of Hartree–Fock and local density‐functional theories. *J. Chem. Phys.* **1993**, *98*, 1372.
53. Schäfer, A.; Huber, C.; Ahlrichs, R. Fully optimized contracted Gaussian basis sets of triple zeta valence quality for atoms Li to Kr. *J. Chem. Phys.* **1994**, *100*, 5829.
54. Chiba, S.; Chen, H. sp^3 C–H oxidation by remote H-radical shift with oxygen- and nitrogen-radicals: a recent update. *Org. Biomol. Chem.* **2014**, *12*, 4051.
55. Wang, Y.; Olankitwanit, A.; Rajca, S.; Rajca, A. Intramolecular hydrogen atom transfer in aminyl radical at room temperature with large kinetic isotope effect. *J. Am. Chem. Soc.* **2017**, *139*, 7144.
56. Elsenbaumer, R. L.; Mosher, H. S. Enantiomerically pure (*R*)-(+)-2-phenylethanol-2-*d* and -1,1,2-d_3, and (*S*)-(+)-1-phenylethane-1-*d*, -1,2,-d_2, -1,2,2-d_3, and -1,2,2,2-d_4. *J. Org. Chem.* **1979**, *44*, 600.
57. Dale, J. A.; Dull, D. L.; Mosher, H. S. α-Methoxy-α-trifluoromethylphenylacetic acid, a versatile reagent for the determination of enantiomeric composition of alcohols and amines. *J. Org. Chem.* **1969**, *34*, 2543.
58. Dale, J. A.; Mosher, H. S. Nuclear magnetic resonance enantiomer regents. Configurational correlations via nuclear magnetic resonance chemical shifts of diastereomeric mandelate, O-methylmandelate, and α-methoxy-α-trifluoromethylphenylacetate (MTPA) esters. *J. Am. Chem. Soc.* **1973**, *95*, 512.
59. White, R. E.; Miller, J. P.; Favreau, L. V.; Bhattacharyya, A. Stereochemical dynamics of aliphatic hydroxylation by cytochrome P-450. *J. Am. Chem. Soc.* **1986**, *108*, 6024.
60. Ishii, S.; Zhao, S.; Helquist, P. Stereochemical probes of intramolecular C–H insertion reactions of iron-carbene complexes. *J. Am. Chem. Soc.* **2000**, *122*, 5897.
61. Alberti, M. N.; Vassilikogiannakis, G.; Orfanopoulos, M. Stereochemistry of the singlet oxygenation of simple alkenes: a stereospecific transformation. *Org. Lett.* **2008**, *10*, 3997.
62. Lang, K.; Torker, S.; Wojtas, L.; Zhang, X. P. Asymmetric induction and enantiodivergence in catalytic radical C–H amination via enantiodifferentiative H-atom abstraction and stereoretentive radical substitution. *J. Am. Chem. Soc.* **2019**, *141*, 12388.